MARMARA UNIVERSITY
FACULTY OF ENGINEERING

DEVELOPMENT OF A PARALLEL ORIENTATION MECHANISM

YUŞA KARAHAN - 150419560

GRADUATION PROJECT REPORT
Department of Mechanical Engineering

Supervisor
Assoc. Prof. Uğur TÜMERDEM

ISTANBUL, 2025

MARMARA UNIVERSITY
FACULTY OF ENGINEERING

Development of a Parallel Orientation Mechanism

by

Yuşa Karahan

June, 2025, Istanbul

SUBMITTED TO THE DEPARTMENT OF MECHANICAL ENGINEERING IN PARTIAL FULFILLMENT OF THE REQUIREMENTS FOR THE DEGREE

OF

BACHELOR OF SCIENCE

AT

MARMARA UNIVERSITY

Signature of Author(s) .....

Department of Mechanical Engineering

Certified By .....

Project Supervisor, Department of Mechanical Engineering

Accepted By.....

Head of the Department of Mechanical Engineering

ACKNOWLEDGEMENT

First of all, I would like to thank my supervisor Assoc. Prof. Uğur TÜMERDEM, for the valuable guidance and advice on preparing this thesis and giving me moral and material support.

July, 2025 Yuşa Karahan

CONTENTS

ABSTRACT

Optimization of Space Bar Structures Using Hybrid Model of Artificial Neural Network and Simulated Annealing

Parallel orientation mechanisms, also known as wrist mechanisms, are kinematic structures used particularly in robotics and industrial automation for applications requiring precise positioning and orientation. Thanks to their parallel kinematic structure, they minimize positional errors while increasing load-bearing capacity. The mechanism has been optimized for 3 degrees of freedom (roll, pitch, yaw), making it suitable for fields requiring precise orientation, such as industrial automation, robotic surgery, and space positioning systems. With Industry 4.0, its use has been increasing, especially in micro-assembly and robotic surgery applications.

In this thesis, a study has been conducted on the design of a parallel mechanism with 3 degrees of freedom. In this mechanism, three independent arms are connected in parallel between a fixed base and a moving platform. Each arm has an RSR (Revolute-Spherical-Revolute) joint structure. Additionally, there is a connection with a UUP (Universal-Universal-Prismatic) joint structure between the centers of the fixed base and the moving platform. This connection enables a screw motion along its own axis, providing roll movement due to the motion of the moving platform.

The goal of this project is to enable the mechanism to perform 90-degree rotation in the pitch and yaw axes and 360-degree roll motion using three motors located on the base. The mechanism was designed using SolidWorks, and kinematic analysis was performed to derive the kinematic equations.

Furthermore, the designed mechanism was manufactured using a 3D printer. The produced parts were assembled, bringing the mechanism designed in SolidWorks to life.

SYMBOLS

Symbol	Quantity	Unit
α	: Pitch angle	deg
β	: Yaw angle	deg
Υ	: Screw angle	deg
θ_i (i=1,2,3)	: Link angles	deg
r	: Radial distance	mm
$\hat{n}_P$	: Orientation vector	
M_i (i=1,2,3)	: Midplane points	
K_i (i=1,2,3)	: Fixed points of the bottom platform	
s_i (i=1,2,3)	: sine	
c_i (i=1,2,3)	: cosine	
$\hat{n}_B$	: Base platform unit vector	
P	: Center point of the top platform	
${}^{B}T$	: Transformation matrix from base to top platform	
r_0	: Initial thrust distance	mm
Δr	: Displacement in thrust axis	mm
φ	: Total orientation angle (pitch and yaw)	deg
φ_1	: Center leg bending angle 1	deg
φ_2	: Center leg bending angle 2	deg
l_i (i=1,2,3)	: Lenght parameters of center leg	mm
Δd	: Displacement of the screw motion	mm
h	: Displacement of the screw motion	mm
p	: Pitch of screw	mm

ABREVIATIONS

DOF :Degree of Freedom

MATLAB :Matrix Laboratory

NATO :North Atlantic Treaty Organization POM :Parallel Orientation Mechanism

PRR :Prismatic-Revolute-Revolute

PU :Prismatic- Universal

RRR :Revolute-Revolute-Revolute

RSR :Revolute-Spherical-Revolute SGR :Security Guard Robot

SPS :Spherical- Prismatic- Spherical

UUP :Universal-Universal-Prismatic

LIST OF FIGURES

LIST OF TABLES

1. INTRODUCTION

Orientation mechanisms are critical components in various engineering applications, enabling precise angular positioning and alignment of objects or tools. These mechanisms are widely used in robotics, aerospace, manufacturing, and biomedical systems, where accurate control of orientation is essential. Traditional serial orientation mechanisms, which rely on a series of interconnected joints, often face limitations such as reduced stiffness, cumulative errors, and limited payload capacity. To overcome these challenges, parallel orientation mechanisms have been developed as an alternative solution.

Parallel orientation mechanisms utilize multiple kinematic chains connected between a fixed base and a moving platform, offering advantages such as higher stiffness, greater precision, and improved load distribution. Due to their closed-loop structure, these mechanisms can achieve better dynamic performance and accuracy compared to their serial counterparts. Common applications include flight simulators, telescope positioning systems, surgical robots, and precision machining equipment.

1.1 History of Orientation Mechanisms in Robotics

In the parallel kinematics community, Pollard's parallel robot is well known as the first industrial parallel robot design. This ingenious invention represents a five-DOF three-branched parallel robot. In this parallel robot, three proximal arms are pivoted by rotary motors fixed to the base, and three distal arms are connected to the three proximal arms via universal joints. Two of the distal arms are connected to the third via ball joints, while a tool head is connected to the third distal arm via a universal joint. Thus, the three motors determine the position of the tool head, while its orientation is controlled by two other motors fixed at the base and transmitting the motion to the tool head via flexible rotary cables. Pollard's parallel robot was intended for spray painting but, unfortunately, was never built.

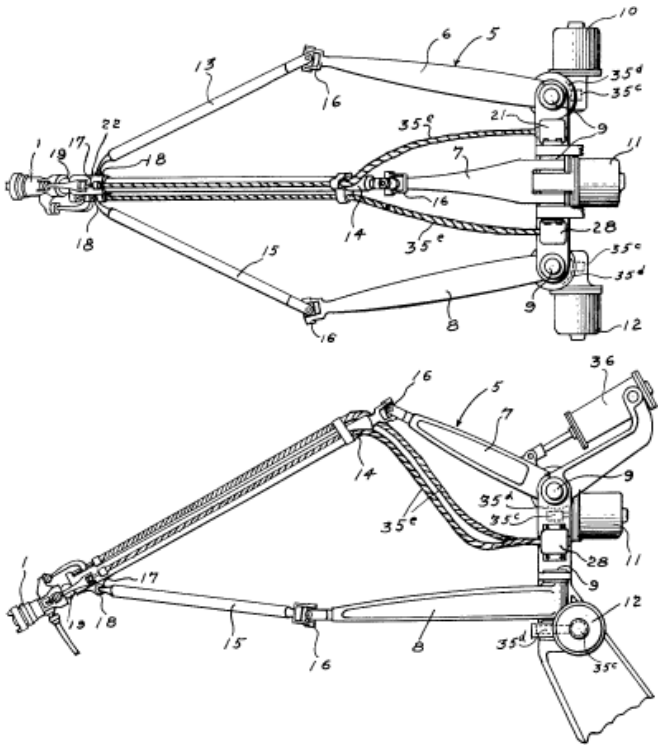

Figure 1.1. The first spatial industrial parallel robot, patented in 1942 (US Patent No. 2,286,571).

The origin of parallel kinematic mechanisms in modern applications dates back to the experimental tire testing apparatus developed by Eric Gough in the late 1940s. This system represents the first example of a 6-degree-of-freedom parallel mechanism, designed to characterize the mechanical behavior of automotive tires under multi-axial loading. Controlled by six independent hydraulic actuators, the platform successfully simulated complex load combinations, leveraging its advantages of high stiffness and force capacity. However, the technological limitations of the era highlighted significant drawbacks, including mechanical complexity, a limited workspace, and control challenges. Gough's pioneering work established a lasting legacy in industrial testing systems, particularly by laying the conceptual foundation for the Stewart Platform.

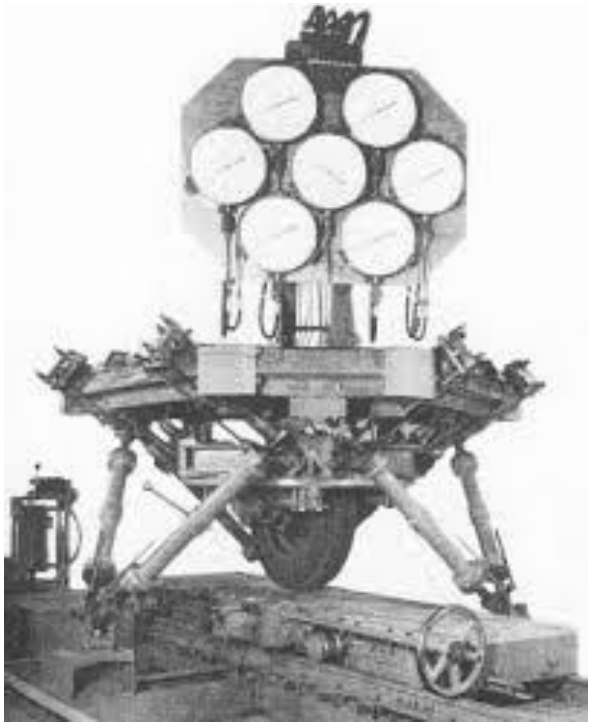

Figure 1.2. The first octahedral hexapod or the original Gough platform at birth in 1954 (Proc. IMechE, 1965-66)

In 1965, D. Stewart published the seminal paper "A Platform with Six Degrees of Freedom" in Philosophical Transactions of the Royal Society, which standardized parallel mechanisms in academic literature. In this work, Stewart proposed a parallel kinematic structure specifically optimized for flight simulators. The platform's high load-bearing capacity, superior stiffness, and dynamic performance advantages drew significant attention in military and civil aviation applications. However, the computational complexity of its inverse kinematic solutions, singularity problems, and orientation angle limitations were documented as major design challenges. Stewart's model established a universal reference point for modern hexapod systems.

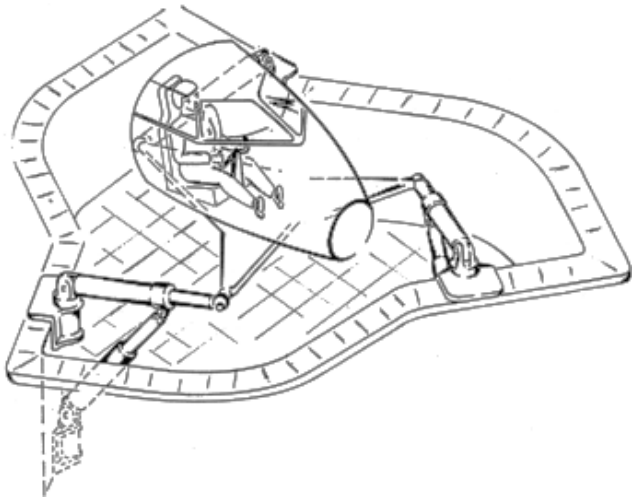

Figure 1.3. Schematic of the one and only "Stewart platform" (Proc. IMechE, 1965-66).

Following Stewart's theoretical framework, Klaus Cappel played a critical role in transferring parallel kinematic mechanisms to industrial applications. His 1967 U.S. Patent 3,295,224 ("Motion Simulator") detailed a practical configuration of a six-degree-of-freedom parallel platform, paving the way for commercial use, particularly in flight simulators. Cappel's design was integrated into military flight training systems by the Singer-Link company, becoming a long-standing standard in the field.

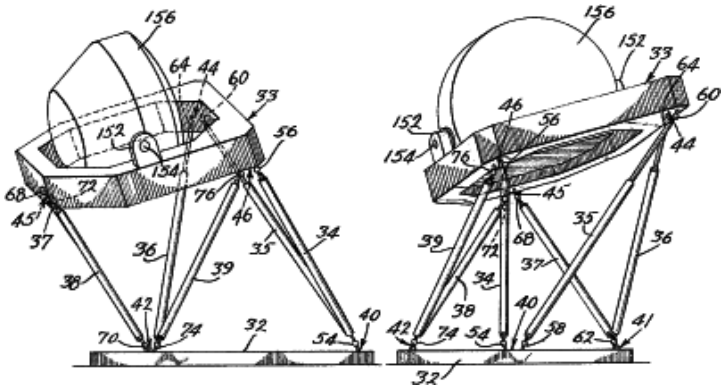

Figure 1.4. Excerpt from the first patent on an octahedral hexapod issued in 1967 (US patent No. 3,295,224).

Cappel's work contributed significantly to the dynamic performance optimization and mechanical reliability of parallel mechanisms. Merlet (2006) emphasizes that although Cappel's configurations were developed independently of the Stewart platform, they were adopted by industry due to their advantages in high load capacity and repeatability. However, the system's limited workspace and the complexity of hydraulic actuation were noted as key disadvantages due to the technological constraints of the time.

Cappel's contributions served as a bridge in the transition of parallel kinematic mechanisms from theory to industrial applications and laid the foundation for modern motion simulation

systems. These design principles, used for decades in military and civil aviation, remain a reference for modern hexapod-based simulators today.

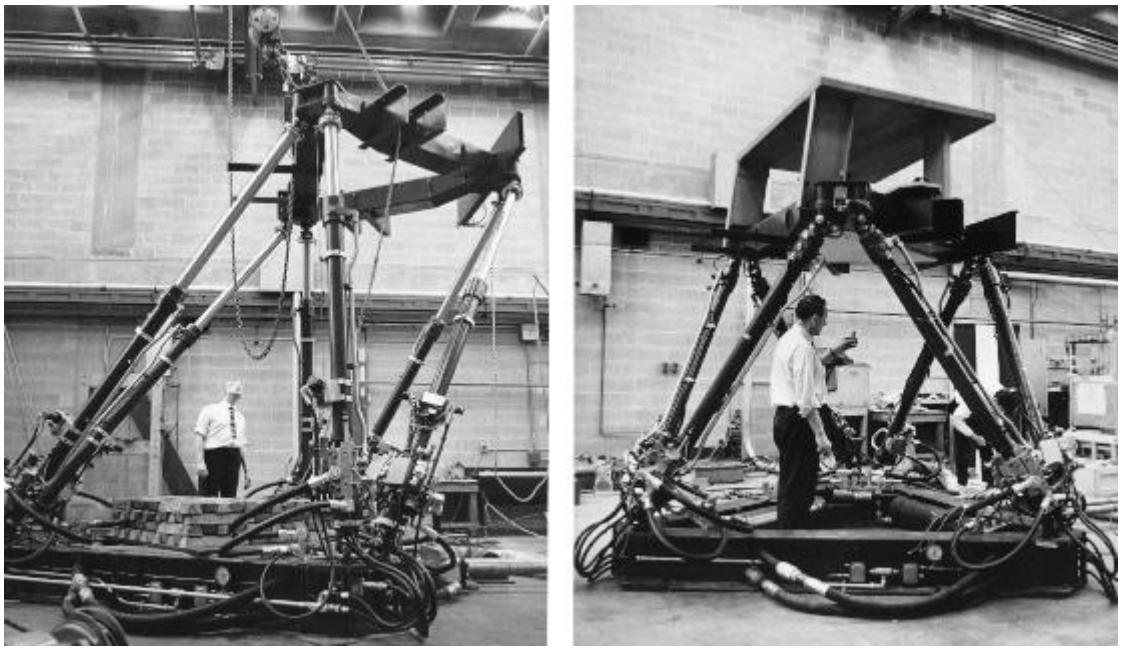

Figure 1.5. The first flight simulator based on an octahedral hexapod as in the mid-1960s (courtesy of Klaus Cappel).

Introduced in 1994 by Giddings & Lewis, the Variax went down in history as the first commercial parallel kinematic machine tool for industrial manufacturing. This system offered a radical performance leap compared to traditional serial CNC machines, standing out with advantages such as superior cutting rigidity, dynamic stability, and multi-axis machining flexibility. The machine demonstrated exceptional capabilities, particularly in machining complex aerodynamic surfaces. However, its commercial success was limited due to drawbacks like high investment costs, complex calibration procedures, and a restricted workspace. Despite these challenges, the experience gained from Variax played a pivotal role in triggering the development of parallel-serial hybrid robots like Tricept and Exechon, which have since become indispensable in modern aerodynamic component manufacturing.

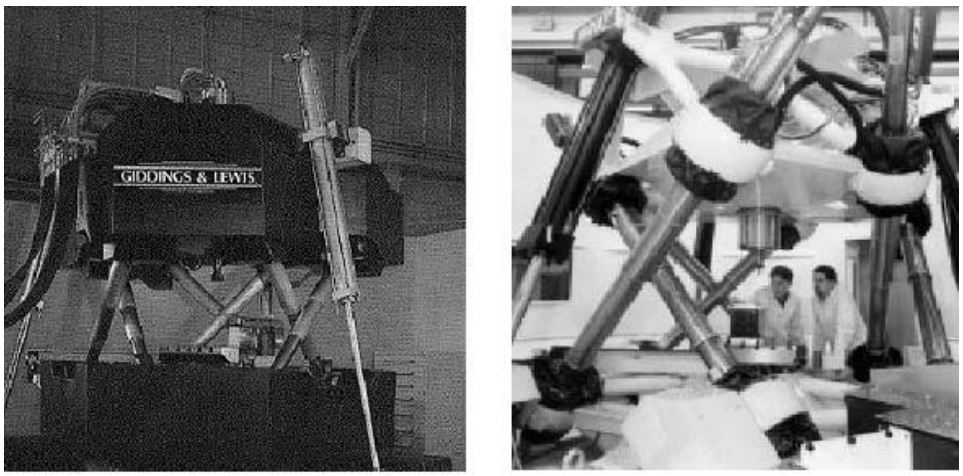

Figure 1.6. The Variax of Gidding and Lewis, the first industrial parallel milling machine presented in 1994 at IMTS [Merlet 2006]

Launched in 1999 by Intuitive Surgical, the da Vinci Robotic Surgical System is regarded as one of the most significant medical applications of parallel kinematics. The system provides unprecedented precision in minimally invasive surgeries, surpassing the physical limits of the human hand with its 7 degrees of freedom, tremor filtering, and 3D visualization capabilities.

Figure 1.7. da Vinci Robotic Surgical System

Particularly effective in complex procedures like prostatectomies and cardiac surgeries, the da Vinci has improved clinical success rates. However, its widespread adoption initially faced challenges due to high costs, lack of haptic feedback, and the need for specialized training.

Despite these limitations, the da Vinci's groundbreaking innovation paved the way for advanced medical robotics, including robotic neurosurgery systems and radiotherapy positioning robots, shaping the future of precision medicine.

2. MECHANICAL DESIGN OF A 3 DOF PARALLEL ORIENTATION MECHANISM

In this project, the aim is to design a 3-DOF parallel orientation mechanism with a movement structure similar to the human wrist. The intended mechanism is expected to provide pitch, yaw, and roll movements. These movements of the mechanism resemble the motions performed by the human wrist: Flexion/Extension, Radial/Ulnar Deviation, and Pronation/Supination. Specifically, the pitch motion of the mechanism corresponds to Flexion/Extension, the yaw motion to Radial/Ulnar Deviation, and the roll motion to Pronation/Supination.

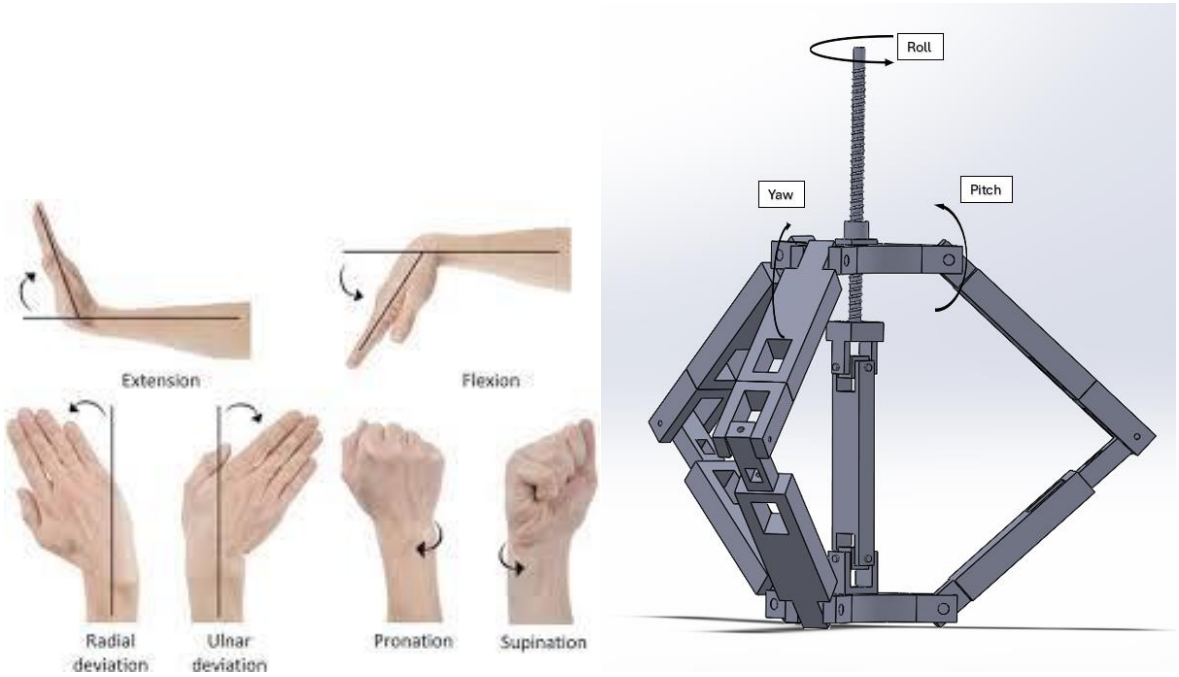

Figure 2.1. DOFs of the human wrist: Flexion, Extension, Deviation, Pronation/Supination. And pitch yaw and roll in mechanism

The 3-degree-of-freedom (3-DOF) parallel orientation mechanism is designed to perform pitch, yaw, and roll motions. The mechanism achieves these movements using three revolute motors located at the base. The orientation motions are realized through the 3-RSR kinematic chains, which converts rotary inputs into the desired rotational outputs.

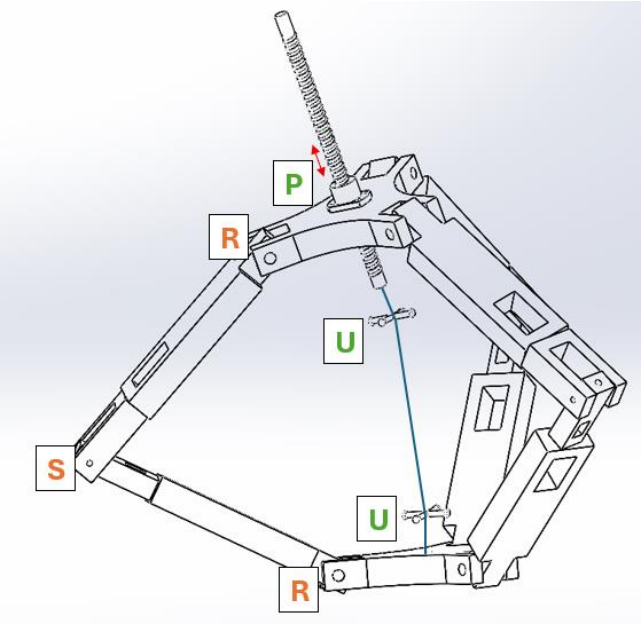

Figure 2.2. The kinematic model of the parallel orientation mechanism RSR and UUP serial chains.

In mechanisms, joints directly affect the workspace, rigidity, and accuracy of the system. They provide degrees of freedom (DOF) between connecting elements and determine the kinematic performance of the mechanism. 3 identical legs which comprise of the mechanism are used symmetrically and each link which is an element of these legs which comprise is connected to each other through revolute joints. To simplify the structure, a combination of 3 revolute joints that are perpendicular to each other can be assumed as a spherical joint.

Table 2.1. Revolute joints

Revolute Joints			
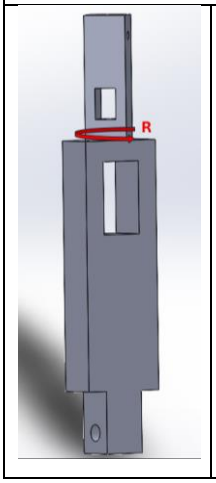	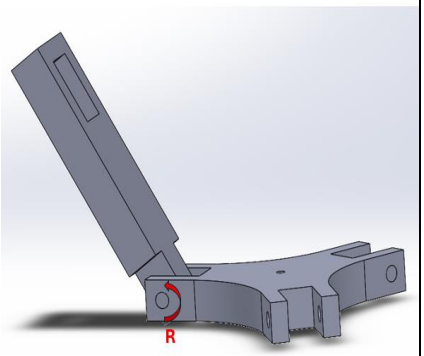	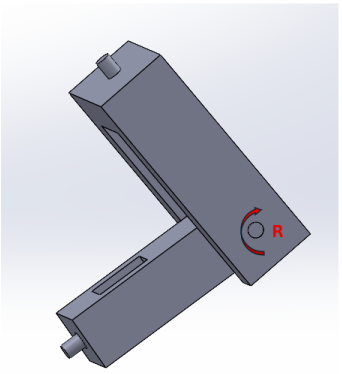	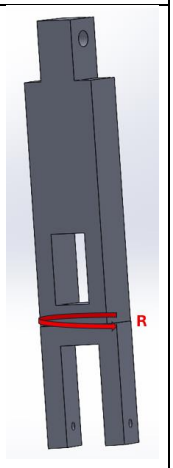

Table 2.2. Universal and prismatic joints

Universal Joint	Prismatic Joint
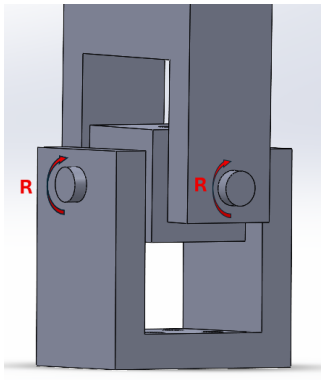	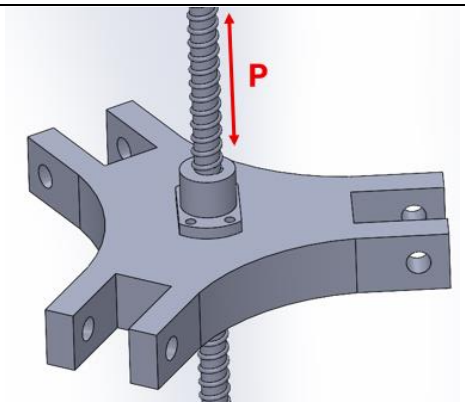

When all joints are assembled, the final configuration of the mechanism is obtained, as shown in Figure 2.3. The lead screw integrated into the UUP (Universal-Universal-Prismatic) linkage is connected to the midpoint of the moving platform. As the mechanism operates, the lead screw enables a $\pm 360°$ rolling motion without requiring an additional motor, thanks to its threaded design. Additionally, the mechanism can perform 2-DOF rotational motion along the pitch and yaw axes, achieving a range of $\pm 90°$ in each direction.

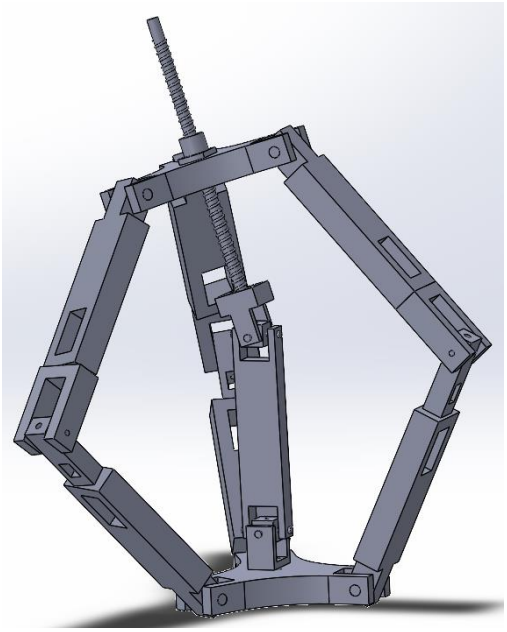

Figure 2.3. Final assembly of mechanism

3. KINEMATIC ANALYSIS

This section formulates the kinematic analysis of the 3-DOF parallel orientation mechanism, comprising two subsections: position kinematics and velocity kinematics.

3.1 Position Kinematic Analysis

The position kinematic analysis involves determining the end-effector's position and orientation as a function of the actuator motions. In position kinematics, the mathematical model of the parallel orientation mechanism consisting of forward and inverse kinematic equations is obtained by using the geometrical constraints. Figure 3.1 shows a general scheme of forward and inverse kinematics. It shows how pitch (α), yaw (β) and screw angle (Υ)are found based on motor angles (θ_i), and vice versa.

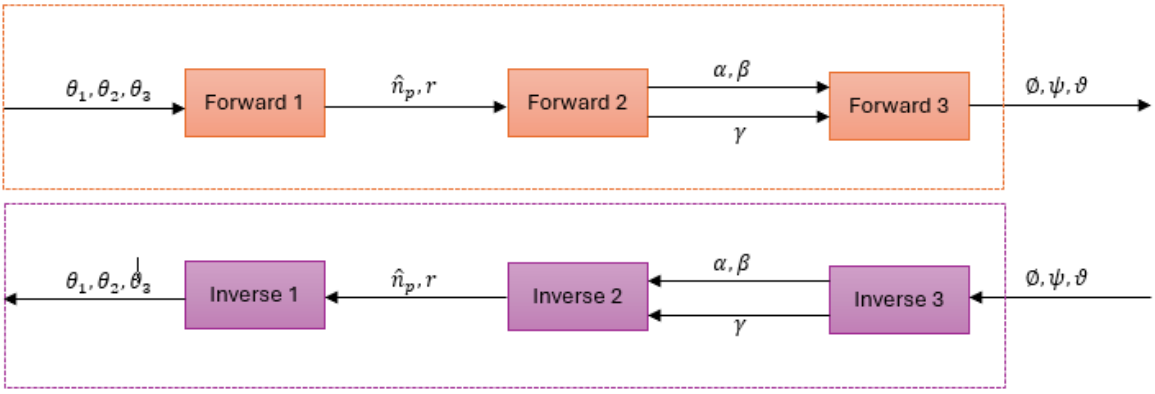

Figure 3.1. Position kinematic analysis steps

3.1.1. Forward Kinematics

Forward kinematic analysis for the parallel orientation mechanism gives pitch (α), yaw (β) and screw angle (Υ). Angles of rotary motors (θ_i) are used as input value.

a) Forward 1

This section computes the tool orientation unit vector ($\hat{\boldsymbol{n}}_{\boldsymbol{p}}$) and radial distance ($r$) from the link angles ($\theta_i$) derived in Forward Kinematics. As illustrated in Figure 3.2, the midplane point ${}^{B}M_i$ is defined vectorially as the sum of ${}^{B}K_i$ (a fixed point on the wrist's base platform) and the displacement vector $F_i^B t_i$.

$$ {}^{B}M_i = {}^{B}K_i + F_i^B t_i \tag{3.1}$$

where F_i is a constant link length and ${}^{B}t_i$ is a unit vector of that $F_i^B t_i$ can be described with respect to θ_i ,

$$ {}^{B}t_i = \begin{bmatrix} s_i \\ -c_i c\emptyset_i \\ -c_i s\emptyset_i \end{bmatrix} \tag{3.2} $$

In $\emptyset_i$ is 180º, 300º and 60º respectively with $s_i = sin\ (\emptyset_i)$ and $c_i = cos(\emptyset_i)$ where $i = 1{:}3$. The unit vector $\hat{u}$ along the distance between the center points of the top and bottom platforms is calculated as follows,

$$ \hat{u} = \frac{\left({}^{B}M_2 - {}^{B}M_1\right) \times \left({}^{B}M_3 - {}^{B}M_1\right)}{\left|\left({}^{B}M_2 - {}^{B}M_1\right) \times \left({}^{B}M_3 - {}^{B}M_1\right)\right|} = \begin{bmatrix} \hat{u}_x \\ \hat{u}_y \\ \hat{u}_z \end{bmatrix} \tag{3.3} $$

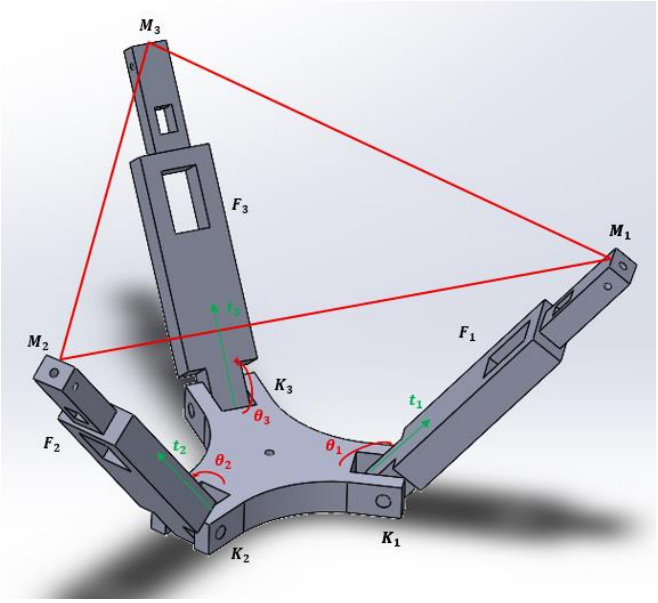

Figure 3.2. Visualization of kinematic structure including vectors and points on the wrist part

As shown in Figure 3.4, thrust distance r is computed by using the relation that $\frac{P}{2}$ is the projection of r onto the unit vector $\hat{u}$:

$$ r = \frac{P}{2\hat{n}_B \cdot \hat{u}} $$

(3.4)

where $\hat{n}_B$ is the is the unit vector perpendicular to the center of the bottom platform ($\hat{\boldsymbol{n}}_{\boldsymbol{B}} = [1 \quad 0 \quad 0]^T$) and P is the distance between the center points of the top and bottom platforms projection of the point which can be computed using the relation that P is the projection of any vertices on midplane $\left({}^{B}M_i\right)$ onto $\hat{u}$ and

$$P = 2\left({}^{B}M_i \cdot \hat{u}\right) \tag{3.5}$$

The tool orientation unit vector $\hat{\boldsymbol{n}}_{\boldsymbol{P}}$ is found using vector summation:

$$\hat{n}_B r + \hat{n}_P r = {}^{B}P \tag{3.6}$$

where ${}^{B}P$ is described as:

$${}^{B}P = \hat{u}P = r\begin{bmatrix} 1 + \hat{n}_{Px} \\ \hat{n}_{Py} \\ \hat{n}_{Pz} \end{bmatrix} \tag{3.7}$$

By substituting (3.4) and (3.5) into (3.6), $\hat{\boldsymbol{n}}_{\boldsymbol{P}}$ is found:

$$\hat{n}_P = \frac{{}^{B}P}{r} - \hat{n}_B \tag{3.8}$$

a) Forward 2

This section presents the analytical derivation of tool bending angles (α, β) and screw displacement, formulated as functions of the tool orientation unit vector $(\hat{n}_P)$ and radial distance (r). The transformation matrix, which encodes both positional and orientational kinematics, is constructed using modified Denavit-Hartenberg (DH) parameters specific to the wrist assembly (Table 3.1). The associated coordinate frame assignment is depicted in Figure 3.3.

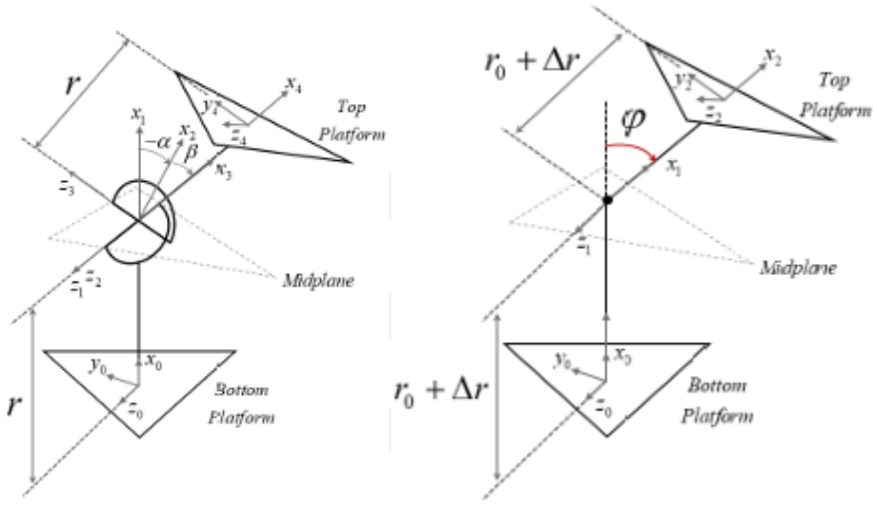

Figure 3.3. The kinematic structure diagrams of the wrist

$$ {}^{B}_{P}T = \begin{bmatrix} c_\alpha c_\beta & -s_\alpha & c_\alpha s_\beta & c_\alpha c_\beta \\ s_\alpha c_\beta & c_\alpha & s_\alpha s_\beta & s_\alpha c_\beta \\ -s_\beta & 0 & c_\beta & s_\beta \\ 0 & 0 & 0 & 1 \end{bmatrix} \tag{3.8} $$

Table 3.1. DH Parameters of the 3 DOF wrist mechanism

i	α_{i-1}	a_{i-1}	d_i	θ_i
1	r	0	0	0
2	1	0	0	α
3	0	$-\pi/2$	0	β
4	r	$-\pi/2$	0	0

Since the up direction is determined as the x-axis, the first column of the matrix given in is $\hat{n}_P$:

$$ \hat{n}_P = \begin{bmatrix} 2\hat{u}_x^2 - 1 \\ 2\hat{u}_x\hat{u}_y \\ 2\hat{u}_x\hat{u}_z \end{bmatrix} = \begin{bmatrix} cos\alpha cos\beta \\ sin\alpha cos\beta \\ -sin\beta \end{bmatrix} = \begin{bmatrix} c_\alpha c_\beta \\ s_\alpha c_\beta \\ -s_\beta \end{bmatrix} \tag{3.9} $$

Thus, α and β can be found,

$$\alpha = \alpha tan2\left(\hat{n}_{P_y}, \hat{n}_{P_x}\right) \tag{3.10}$$

$$\beta = atan2\left(-\hat{n}_{P_z}{}^2 \sqrt{\hat{n}_{P_x}{}^2 + \hat{n}_{P_y}{}^2}\right) \tag{3.11}$$

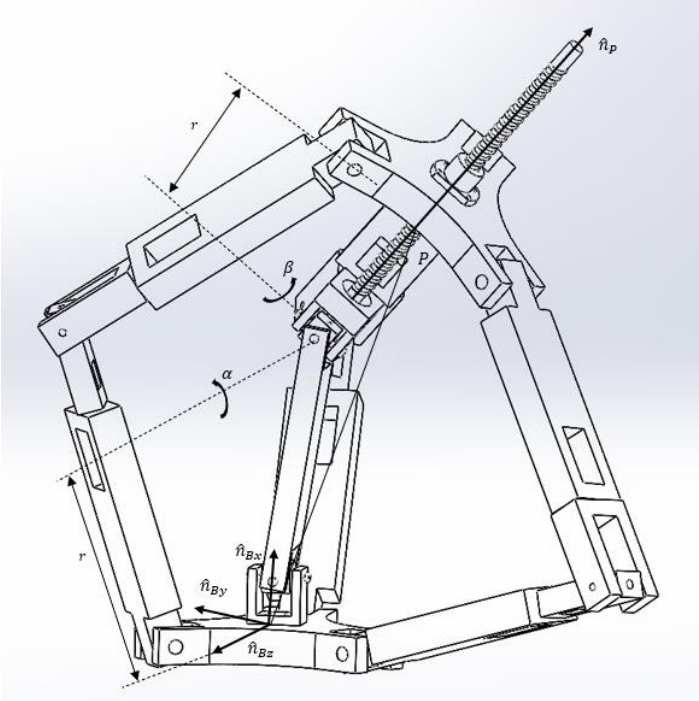

Figure 3.4. Representations of 3 DOF wrist mechanism parameters

$$T_w = \begin{bmatrix} c_\alpha c_\beta & -s_\alpha & c_\alpha s_\beta & (r_0 + \Delta r)(1 + c_\alpha c_\beta) \\ s_\alpha c_\beta & c_\alpha & s_\alpha s_\beta & (r_0 + \Delta r) s_\alpha c_\beta \\ -s_\beta & 0 & c_\beta & -(r_0 + \Delta r) s_\beta \\ 0 & 0 & 0 & 1 \end{bmatrix}$$

(3.12)

The sum of the initial thrust distance r_0 and the change in thrust distance Δr is known as r.

$$r = r_0 + \Delta r$$

(3.13)

The angle φ, derived from the tool orientation angles, is illustrated in Figure 3.5. This angle is calculated as the dot product between the tool unit vector and the normal vector of the bottom platform's central plane.

$$\varphi = \varphi_1 + \varphi_2 = cos^{-1}\left(\frac{\hat{n}_p \cdot \hat{n}_p}{|\hat{n}_p||\hat{n}_B|}\right)$$

(3.14)

Consistent with this approach, the central leg's planar motion is modeled by mapping universal joint displacements to orientation angles $\varphi_1$and φ_2 (Figure 3.5). The kinematic transformation is captured through the following DH matrix derivation:

$${}^{0}_{3}T = \begin{bmatrix} c\varphi_{12} & -s\varphi_{12} & 0 & l_1 + (l_3 + \Delta d)c\varphi_{12} + l_2 c\varphi_1 \\ s\varphi_{12} & c_\alpha & 0 & (l_3 + \Delta d)s\varphi_{12} + l_2 s\varphi_1 \\ 0 & 0 & 1 & 0 \\ 0 & 0 & 0 & 1 \end{bmatrix}$$

(3.15)

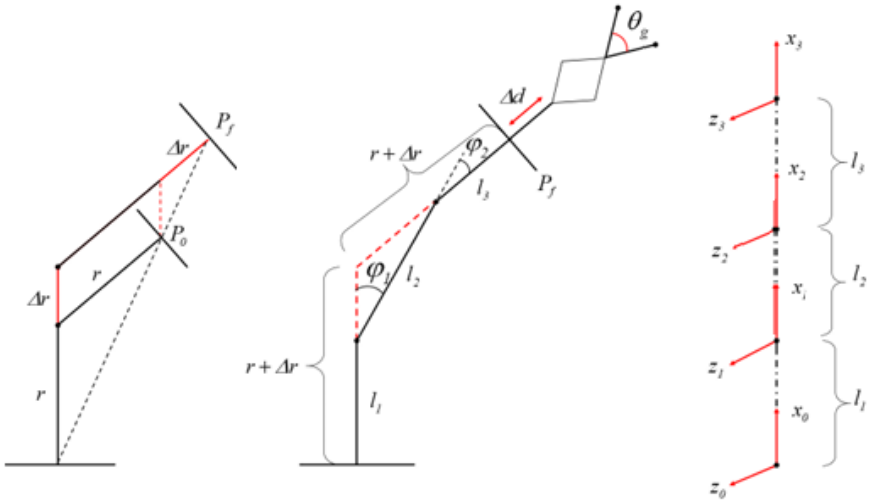

Figure 3.5. Visualization of DH parameters of the center leg

Table 3.2. DH Parameters of the center leg of the wrist mechanism

i	α_{i-1}	a_{i-1}	d_i	θ_i
1	0	l_1	0	φ_1
2	0	l_2	0	φ_2
3	0	$l_3 + \Delta d$	0	β

By applying the conversion α, β to φ :

$$T_w{}' = \begin{bmatrix} c_\varphi & -s_\varphi & 0 & (r_0 + \Delta r)(1 + c_\varphi) \\ s_\varphi & c_\varphi & 0 & (r_0 + \Delta r)s_\varphi \\ 0 & 0 & 1 & 0 \\ 0 & 0 & 0 & 1 \end{bmatrix} \tag{3.16}$$

Equate the elements [4,1] and [4,2] in the (3.15) and (3.16) matrices to find Δd.

$$l_1 + (l_3 + \Delta d)c\varphi_{12} + l_2 c\varphi_1 = (r_0 + \Delta r)(1 + c_\varphi) \tag{3.17}$$

$$(l_3 + \Delta d)s\varphi_{12} + l_2 s\varphi_1 = (r_0 + \Delta r)s_\varphi$$

(3.18)

Thus, Δd that is displacement is found:

$$\Delta d = l_1 - l_3 - (1 + c_\varphi)\left(l_1 - r + \sqrt{\frac{{l_2}^2 - (l_1 - r)^2 s_\varphi}{(1 + c_\varphi)}}\right)$$

(3.19)

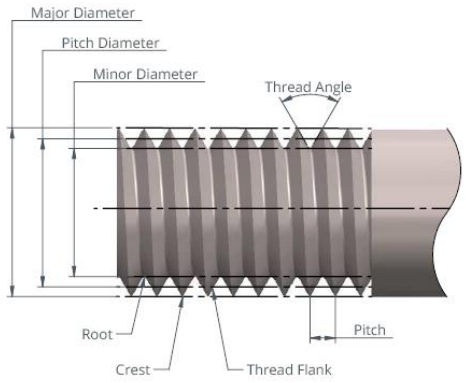

Figure 3.6. End effector screw system details.

In Figure 3.6, we applied the screw type of this mechanism to the inner part of the upper platform with the end effector part. By doing this, we aimed to provide roll motion without additional motor.

$N_t = Number\ of\ turns$

$p = Pitch\ (distance\ between\ threads)$

$h = displacement$

General formula for screw is:

$$h = N_t \cdot p$$

(3.19)

In our mechanism h is not one way and equal to Δd,

$$h = \Delta d$$

(3.19)

If we multiply both sides with 2π,

$$N_t \cdot 2\pi = \left(\frac{\Delta d}{p}\right) \cdot 2\pi$$

(3.20)

By multiplying, number of turns and 2π we find the roll angle using Δd and we call screw roll angle as γ

$$N_t \cdot 2\pi = \gamma \tag{3.21}$$

Finally,

$$\gamma = \left(\frac{\Delta d}{p}\right) \cdot 2\pi \tag{3.22}$$

Δd is found that:

$$\gamma = \left[\frac{l_1 - l_3 - (1 + c_\varphi)\left(l_1 - r + \sqrt{\frac{{l_2}^2 - (l_1 - r)^2 s_\varphi}{(1 + c_\varphi)^2}}\right)}{p}\right] \cdot 2\pi \tag{3.23}$$

b) Forward 3

In this model, the 3-DOF wrist kinematics are described by active pitch (α) and yaw (β) motions, with the roll rotation (γ) being a passive degree of freedom that corresponds to the screw angle (Υ) calculated in the Forward Kinematics formulation (see Forward 2).

Table 3.3. DH Parameters of the 3 DOF wrist including roll axis

i	α_{i-1}	a_{i-1}	d_i	θ_i
1	0	0	r	0
2	0	$-\pi/2$	0	$-\frac{\pi}{2} + \alpha$
3	0	$-\pi/2$	0	$-\frac{\pi}{2} + \beta$
4	0	$-\pi/2$	r	$-\pi/2$

The modified DH parameters are described in Table 3.3 based on the frame assignment with respect to the base frame 0 .The 3 DOF wrist including roll axis of transformation matrix ${}^0_4T$, orientation matrix ${}^0_4R$ and position vector ${}^0P_4$ with respect to the base frame {0} are expressed as:

$$ {}^{0}_{4}T = \begin{bmatrix} c_\alpha & s_\alpha s_\beta & c_\beta s_\alpha & r(c_\beta s_\alpha) \\ 0 & c_\beta & -s_\beta & (-s_\beta) \\ -s_\alpha & c_\alpha s_\beta & c_a & r(c_a) \\ 0 & 0 & 0 & 1 \end{bmatrix} $$

(3.24)

$$ {}^{0}_{4}R = \begin{bmatrix} c_\alpha & s_\alpha s_\beta & c_\beta s_\alpha \\ 0 & c_\beta & -s_\beta \\ -s_\alpha & c_\alpha s_\beta & c_a \end{bmatrix} $$

(3.25)

3.1.2. Inverse Kinematics

a) Inverse 1

Inverse kinematics is used to determine the joint positions that are required to achieve a desired end-effector orientation or position.

$$ R_d = Rot_x(\emptyset) Rot_x(\psi) Rot_z(\vartheta) $$

(3.26)

Where R_d is the desired rotation matrix:

$$ R_d = \begin{bmatrix} R_{11} & R_{12} & R_{13} \\ R_{21} & R_{22} & R_{23} \\ R_{31} & R_{32} & R_{33} \end{bmatrix} $$

(3.27)

$$ \alpha = \alpha tan2\left(-R_{31}, \sqrt{{R_{32}}^2 + {R_{32}}^2}\right) $$

(3.28)

$$ \beta = atan2(R_{13}, R_{33}) $$

(3.29)

$$ \gamma = atan2(R_{21}, R_{11}) $$

(3.30)

b) Inverse 2

In the first step of inverse kinematic analysis, it is required to find $\hat{n}_d$ and r as a function of α, β and γ. It was calculated in the Forward 2 section of $\hat{n}_d$ and it was also shown how it was calculated.

$$ \hat{n}_d = \begin{bmatrix} c_\alpha s_\beta \\ s_\alpha s_\beta \\ -s_\beta \end{bmatrix} $$

(3.31)

When (3.14), (3.17) and (3.18) are arranged and solved according to Δr from three equations, the following equation is obtained.

$$\Delta r = \frac{1}{2}\left(\sqrt{{l_2}^2 + (l_1 - r_0)^2 + (l_1 - r_0)\left(2(-l_1 + r_0)c_\varphi - A_1 + c_{2\varphi}(l_1 - r_0 + A_1)\right)} + l_1 - r_0 - A_1 - c_\varphi(l_1 - r_0 + A_1)\right) \tag{3.32}$$

Where $A_1 = \sqrt{\frac{{l_2}^2 - (l_1 - r)^2 s_\varphi}{\left(1 + c_\varphi\right)^2}}$

$$\Delta d = \frac{2\pi}{\gamma \cdot p} \tag{3.33}$$

$$\gamma = \left[\frac{l_1 - l_3 - \left(1 + c_\varphi\right)\left(l_1 - r + \sqrt{\frac{{l_2}^2 - (l_1 - r)^2 s_\varphi}{\left(1 + c_\varphi\right)^2}}\right)}{p}\right] \cdot 2\pi \tag{3.34}$$

c) Inverse 3

The second step aims to find link angles θ_i with respect to $\hat{n}_p$ and r. To obtain link angles, following equations that associate θ_i and $\hat{n}_p$ are utilized:

$$X_i \cdot \hat{u} = 0 \tag{3.35}$$

$$\frac{P}{2}\hat{u} + X_i = {}^B M_i \tag{3.36}$$

X_i which is a perpendicular vector to $\hat{u}$, starts at the center point of ${}^B P$ and ends at ${}^B M_i$ as can be seen in Figure 3.4.

The constraint equation in (3.28),(3.29),(3.30) is obtained by substituting (3.26) into (3.27),

$$\left({}^B M_i - \frac{{}^B P}{2}\hat{u}\right)\hat{u} = 0 \tag{3.37}$$

And $\hat{u}$ is defined as:

$$\hat{u} = \frac{{}^B P}{\left|{}^B P\right|} \tag{3.38}$$

Substituting (3.1),(3.6) and (3.26) into (3.27), a set of 3 equations depending on θ_i for 3 identical legs composed of RSR joints,

$$X_i c_i + Y_i s_i + Z_i = 0 \tag{3.39}$$

Then, $\theta_i$values can be computed by,

$$\theta_i = 2tan^{-1}\left(\frac{-Y_i \pm \sqrt{{Y_i}^2 - {Z_i}_i{}^2 + {X_i}^2}}{Z_i - X_i}\right) \tag{3.40}$$

3.2 Velocity Kinematic Analysis

Position kinematic analysis is used to generate velocity kinematic analysis of a robot,

$$v = J(q)\omega \tag{3.41}$$

where v is the output velocity vector and ω is the input velocity vector mapped into v by the Jacobian matrix J.

i. Jacobian Analysis

Time derivatives of forward kinematic equations can be used to find the mechanism's Jacobian matrix, which maps the link between actuator velocity and tool tip velocity. The first step is to find the Jacobian matrix of the wrist part. With respect to link angles, tool unit vector of the top platform and thrust distance are differentiated.

$$v = J(q)\omega \tag{3.41}$$

where v is the output velocity vector and ω is the input velocity vector mapped into v by the Jacobian matrix J.

ii. Jacobian Analysis

Time derivatives of forward kinematic equations can be used to find the mechanism's Jacobian matrix, which maps the link between actuator velocity and tool tip velocity. The first step is to find the Jacobian matrix of the wrist part. With respect to link angles, tool unit vector of the top platform and thrust distance are differentiated.

$$J_w = \begin{bmatrix} \frac{\partial \hat{n}_{py}}{\partial \theta_1} & \frac{\partial \hat{n}_{py}}{\partial \theta_2} & \frac{\partial \hat{n}_{py}}{\partial \theta_3} \\ \frac{\partial \hat{n}_{pz}}{\partial \theta_1} & \frac{\partial \hat{n}_{pz}}{\partial \theta_2} & \frac{\partial \hat{n}_{pz}}{\partial \theta_3} \\ \frac{\partial r}{\partial \theta_1} & \frac{\partial r}{\partial \theta_2} & \frac{\partial r}{\partial \theta_3} \end{bmatrix} \tag{3.42}$$

For the second step, J_T is determined by transforming the tool unit vector-thrust distance to the tool orientation angles-thrust distance.

$$J_T = \begin{bmatrix} & T_{2\times 2} & \begin{matrix} 0 \\ 0 \end{matrix} \\ 0 & 0 & 1 \end{bmatrix} \tag{3.43}$$

where $T_{2\times 2}$ enables to transform $\{\hat{n}_{py}, \hat{n}_{pz}\}$ to $\{\alpha, \beta\}$.

For the third step, in up and down motion, the thrust distance and the linear displacement are both determined.

$$J_{\Delta d} = \begin{bmatrix} 1 & 0 & 0 \\ 0 & 1 & 0 \\ \frac{\partial \Delta d}{\partial \alpha} & \frac{\partial \Delta d}{\partial \beta} & \frac{\partial \Delta d}{\partial r} \end{bmatrix} \tag{3.44}$$

Finally, J_Y is calculated using the linear displacement in up and down motion as well as the screw roll angle.

$$J_Y = \begin{bmatrix} 1 & 0 & 0 \\ 0 & 1 & 0 \\ 0 & 0 & \frac{\partial \gamma}{\partial \Delta d} \end{bmatrix} \tag{3.45}$$

It is shown in the following equation how to get from the motor velocities to wrist end effector velocities:

$$\begin{bmatrix} \dot{\alpha} \\ \dot{\beta} \\ \dot{r} \end{bmatrix} = J_T J_w \begin{bmatrix} \dot{\theta}_1 \\ \dot{\theta}_2 \\ \dot{\theta}_3 \end{bmatrix} \tag{3.46}$$

The following step shows how to transform a change in thrust distance into a change in screw roll angle:

$$\begin{bmatrix} \dot{\alpha} \\ \dot{\beta} \\ \dot{\gamma} \end{bmatrix} = J_\gamma J_{\Delta d} \begin{bmatrix} \dot{\alpha} \\ \dot{\beta} \\ \dot{r} \end{bmatrix} \tag{3.47}$$

The total Jacobian of the 3 DOF system is the combining (3.47) and (3.46), the overall Jacobian matrix J can be defined as follows, and the Jacobian matrix is derived by directly differentiating the mechanism's kinematic equations.

$$J = J_\gamma J_{\Delta d} J_T J_w$$

4. MANUFACTURABILITY

The mechanism designed in SolidWorks was manufactured using a 3D printer. Before proceeding to production, the mechanism was dimensioned. During the dimensioning process, the THK BNK0810 coded lead screw used in the mechanism was taken as a reference. The dimensions of the parts constituting the mechanism were determined to maximize the movement of the lead screw. Additionally, the thicknesses of the parts were set to maximize the mechanism's working area. While dimensioning, it was ensured that the parts would not bend or break under operational conditions.

After determining the dimensions of the mechanism parts, the assembly method was carefully planned. During this stage, attention was given to ensuring a modular design for the components. Additionally, the parts were assembled in a way that allows smooth movement of the mechanism.

Table 4.1 bolts used in the mechanism

Bolts			
Diameter:3mm Length:15mm	Diameter:3mm Length:30mm	Diameter:4mm Length:50mm	Diameter:8mm Length:50mm
			

For assembly, bolts with diameters of 3mm, 4mm, and 8mm were used. The holes for these bolts were designed during the modeling phase to facilitate easy assembly while ensuring unrestricted motion of the mechanism.

A universal joint (U-joint) design has been developed for the UUP (universal-universal-prismatic) connection of the mechanism. The design is shown below.

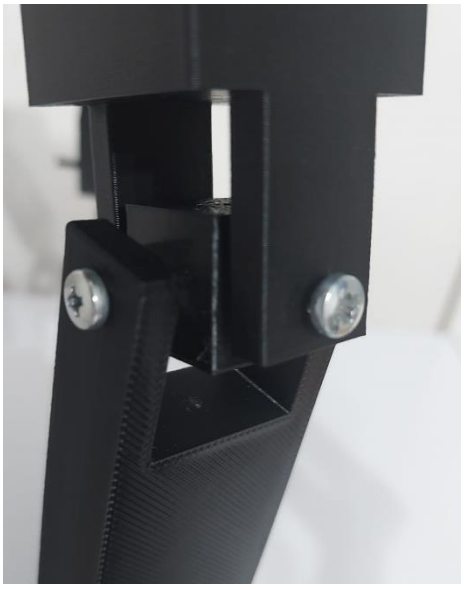

Figure 4.1. Universal joint

Finally, the 3D-printed parts were assembled. Due to the 3D printer's limitations in producing perfectly circular bolt holes, the holes were post-processed to ensure a proper fit for the bolts.

The fully assembled mechanism is shown below.

Figure 4.2. 3-DOF parallel orientation mechanism

5. CONCLUSION

This project successfully designed and prototyped a 3-DOF parallel orientation mechanism using 3D printing technology, demonstrating its feasibility for real-world applications. The mechanism was developed to overcome common limitations in parallel robotics, such as restricted motion range and high costs, by utilizing an innovative kinematic structure with three revolute motors and an integrated screw-driven roll mechanism.

A key achievement of this work was the functional 3D-printed prototype, which validated the mechanical design and assembly process. The use of additive manufacturing allowed for rapid iteration, cost-effective production, and customization of components, ensuring a lightweight yet durable structure. The prototype confirmed the mechanism's ability to achieve ±90° in pitch and yaw and ±360° in roll, meeting the project's objectives for a wide and flexible workspace.

The kinematic analysis provided a solid theoretical foundation, ensuring smooth motion and singularity-free operation. While the focus was on mechanical implementation, future work could explore integrating sensors and control systems to enhance precision and autonomy. Additionally, further optimizations in material selection and joint reinforcement could improve durability for industrial applications.

REFERENCES

- MERLET, Jean-Pierre; GOSSELIN, Clément. Parallel Mechanisms and Robots. 2008.
- PATEL, Y. D., et al. Parallel manipulators applications a survey. Modern Mechanical Engineering, 2012, 2.03: 57.
- TAGHIRAD, Hamid D. Parallel robots: mechanics and control. CRC press, 2013.
- MERLET, Jean-Pierre. Parallel robots. Springer Science & Business Media, 2005. pages 5-11.
- LIU, Kai; FITZGERALD, John M.; LEWIS, Frank L. Kinematic analysis of a Stewart platform manipulator. IEEE Transactions on industrial electronics, 1993, 40.2: 282-293.
- REY, L.; CLAVEL, R. The delta parallel robot. In: Parallel Kinematic Machines. Springer, London, 1999. p. 401-417.
- UZUNOVIC, Tarik, et al. Configuration space control of a parallel Delta robot with a neural network based inverse kinematics. In: 2013 8th International Conference on Electrical and Electronics Engineering (ELECO). IEEE, 2013. p. 497-501.
- SICILIANO, Bruno. The Tricept robot: Inverse kinematics, manipulability analysis and closed-loop direct kinematics algorithm. Robotica, 1999, 17.4: 437-445
- GOSSELIN, Clément M.; HAMEL, J.-F. The agile eye: a high-performance three- degree-of-freedom camera-orienting device. In: Proceedings of the 1994 IEEE international conference on robotics and automation. IEEE, 1994. p. 781-786.
- BONEV, Ilian A.; CHABLAT, Damien; WENGER, Philippe. Working and assembly modes of the Agile Eye. In: Proceedings 2006 IEEE International Conference on Robotics and Automation, 2006. ICRA 2006. IEEE, 2006. p. 2317-2322.
- M. Bazman, N. Yilmaz, and U. Tumerdem, “Dexterous and back-drivable parallelrobotic forceps wrist for robotic surgery,” Proc. - 2018 IEEE 15th Int. Work. Adv.Motion Control. AMC 2018, pp. 153–159, 2018.

- N. Yilmaz, M. Bazman, and U. Tumerdem, “External Force/Torque Estimation on a Dexterous Parallel Robotic Surgical Instrument Wrist,” 2018 IEEE/RSJ Int. Conf. Intell. Robot. Syst., pp. 4396–4403, 2019.
- A. Alassi, N. Yilmaz, M. Bazman, B. Gur, and U. Tumerdem, “Development and kinematic analysis of a redundant, modular and backdrivable laparoscopic surgery robot,” IEEE/ASME Int. Conf. Adv. Intell. Mechatronics, AIM, vol. 2018-July, pp. 213–219, 2018.